Optimal approach to rotational state reconstruction of linear molecules

Qin Xiao(覃 晓)[a)b)] and Gao Jun-Yi(高军毅)[a)†]

[a)] *Wuhan Institute of Physics and Mathematics, Chinese Academy of Sciences, Wuhan* 430071, *China*
[b)] *Graduate University of the Chinese Academy of Sciences, Beijing* 100049, *China*

(Received 10 July 2010; revised manuscript received 25 August 2010)

We present a simulation for the reconstruction of the rotational quantum state of linear molecules to retrieve the density matrix. An optimal approach in the sense of minimal error limit is proposed, in which a variable set of angular frequency is properly chosen and the least square inversion is then applied. This approach of reconstruction from time-dependent molecular-axis angular distribution is proved adaptable for various object states, which has a good numerical stability independent of the selected rotational space.

Keywords: state reconstruction, molecular rotation

PACS: 03.65.Wj, 33.20.Sn **DOI:** 10.1088/1674-1056/20/1/010306

1. Introduction

The experimental measurement of molecular quantum states has gradually come into reality during recent years. Femtosecond time-resolved pump-probe technique provides the ability to detect the ultrafast evolution of such micro systems, as well as their quantum states. For example, the vibrational motion for molecular iodine is reconstructed[1] from ion images, and the shape of the highest occupied molecular orbital is determined by measuring the harmonic emission from aligned molecules.[2] To reconstruct a pure wavefunction of molecular rotation for the first time, an experiment has been carried out[3] using a complicated pump-manipulate-probe scheme.

For a general mixed state of molecular rotation, methods have also been proposed[4,5] to reconstruct its density matrix. The proposal in Ref. [4] suggests that states in a rotational subspace with a fixed magnetic number could be retrieved from data of laser pump-probe ion images, i.e. time-dependent molecular-axis angular distribution (TDMAD).

However, the feasibility and adaptivity of such a method has not been checked, as these properties are related to whether the observable is sensitive to the object state, and also to the condition of reconstruction approach. The method in Ref. [5] is revealed as extremely ill-conditioned for a slightly larger space, despite the fact that many choices of observation were tested and the application of pseudoinverse was made. It is similar here that the reconstruction cannot be achieved only by tomography in this rotational subspace, and the matrix inverse must be employed. Therefore, we perform a numerical reconstruction in dealing with simulated data of TDMAD, and establish a specific approach for the purpose of minimal error by taking all the information of the observable into account.

In this paper, the related quantum mechanics is outlined and a deterministic reconstruction approach with the optimisation process is established in Section 2. In Section 3, an example of retrieving the rotational quantum state of molecular nitrogen is demonstrated, and a series of object states in different rotational subspaces are tested for the convergence of this approach. The numerical condition of the inversion procedure is investigated in Section 4 and the effect from centrifugal distortion is discussed as well.

2. Simulation frame

2.1. Quantum mechanics calculation

A quantum simulation (e.g. see Refs. [6] and [7]) is employed to calculate the prepared rotational state $\hat{\rho}_{\rm pre}$ and the observable TDMAD in a non-resonant femto-second laser pump-probe scheme of rotational excitation (for instance, the effect of laser-induced molecular alignment[8]).

The molecular rotation is manipulated by a moderately intense laser, and the total Hamiltonian is

$$\hat{H} = \hat{H}_0 + \boldsymbol{\varepsilon} \cdot \boldsymbol{\mu}. \tag{1}$$

†Corresponding author. E-mail: gaojunyi@wipm.ac.cn

© 2011 Chinese Physical Society and IOP Publishing Ltd

Non-adiabatic interaction between laser field $\boldsymbol{\varepsilon}$ and the induced molecular dipole moment $\boldsymbol{\mu}$ leads to Raman-type transition and produces a rotationally-broad coherent wave packet in the molecular ensemble.

On the bases of spherical harmonics,[9] the evolution of the rotational wavefunction and the prepared density matrix are received by numerically solving the nonperturbative time-dependent Schrodinger equation

$$\begin{aligned} &\mathrm{i}\hbar\frac{\partial|\Psi\rangle}{\partial t} = \hat{H}|\Psi\rangle, \\ &|\Psi\rangle = \sum_{JM} C_{JM}\,\mathrm{e}^{(E_J/\mathrm{i}\hbar)t}|JM\rangle, \end{aligned} \tag{2}$$

with J being the rotational angular momentum and M its projection along the external field direction.

The basic condition of the pump-probe scheme in the calculation is stated as follows. The initial population of the rotational state of the linear molecular nitrogen is assumed to contain a major objective part $|J_0M_0\rangle = |51\rangle$ with 10% incoherent impurity $|J_0M_1\rangle = |54\rangle$. A linear polarised non-resonant laser pulse is used for rotational excitation, with a peak intensity $I = 4\times10^{13}$ W/cm^2 and a duration 100 fs. After certain time-delay, an ultrashort probe pulse (with an intensity one order higher than the pump) induces double ionisation, followed by Coulomb explosion,[10] where the probe rate is roughly connected to the laser intensity by the tunneling ionisation model MO-ADK.[11] Assume that the probe pulse is short enough to neglect its reorientation,[12] so the direction of ion fragments represents the orientation of molecular axis in the probe instant. In the excitation by a linearly polarised laser, the fragments are homogeneously distributed among azimuthal angles, and TDMAD (data are shown in Fig. 1)

$$R(\Omega,t) = \langle\Omega|\hat{\rho}(t)|\Omega\rangle \tag{3}$$

is recorded by e.g, the ion imaging.

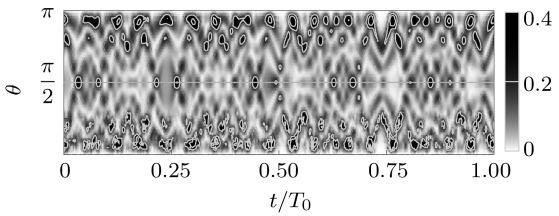


Fig. 1. The gray level density plot of TDMAD. The upper half $\theta \in [\pi/2, \pi]$ is obtained from quantum mechanics calculation, with implied $J_{\max} = 20$ deciding the original sampling. Random noise is added on in the lower half $\theta \in [0, \pi/2]$ for illustration. Unity of the distribution is achieved by integral over 4π solid angle.

Gaussian-type random noise with relative strength of $\eta = 1/2$ is added to this original single detection. The sampling of the quasi-periodic observable contains a full cycle in the range $t \in [0, T_0]$, with $T_0 = 1/2Bc \approx 8.35$ps the rotational period (B is the rotational constant), and $\theta \in [0, \pi]$. For practical excitation under a certain cutoff angular momentum $J_{\max}$, the sample numbers are chosen by Shannon's theorem $N_t \geq J_{\max}(J_{\max}+1)$ and $N_\theta \geq 2J_{\max}$.

2.2. Reconstruction formulae

The elementary reconstruction process is similar to the idea given in Ref. [4], and we are devoted to the exploration of the furthest usable information from TDMAD, and then construct an optimal reconstruction approach. With a single magnetic number M_0 and its conservation in the excitation, the object density matrix confined in angular momentum J space is

$$\rho_{J_1J_2} = \langle J_1M_0|\hat{\rho}(0)|J_2M_0\rangle, \tag{4}$$

which is defined at $t = 0$, the moment of the end of the pump pulse. TDMAD is linearly related to density matrix elements

$$\begin{aligned} &R(\Omega,t) \\ &= \sum_{J_1J_2} \mathrm{e}^{((E_{J_1}-E_{J_2})/\mathrm{i}\hbar)t} Y_{J_1M_0}(\Omega) Y^*_{J_2M_0}(\Omega)\rho_{J_1J_2}. \end{aligned} \tag{5}$$

Two independent variables α and β corresponding respectively to angular and temporal frequencies are introduced in the tomography

$$\begin{aligned} &S(\alpha,\beta) \\ &= \frac{1}{T_0}\iint \mathrm{d}\,\Omega \int_0^{T_0} R(\Omega,t)\,\mathrm{e}^{-(\pi\beta/\mathrm{i}T_0)t} Y_{\alpha0}(\Omega)\,\mathrm{d}t. \end{aligned} \tag{6}$$

By combining the above two equations, a theoretical expression is obtained

$$\begin{aligned} S(\alpha,\beta) = &\sum_{J_1J_2}(-1)^{M_0}\sqrt{\frac{(2J_1+1)(2J_2+1)}{4\pi(2\alpha+1)}} \\ &\times \langle J_1M_0J_2 - M_0|\alpha\,0\rangle \\ &\times \langle J_10J_20|\alpha\,0\rangle\delta(\beta,\beta'_{J_1J_2})\rho_{J_1J_2}. \end{aligned} \tag{7}$$

In the rigid rotor approximation $E_J \sim BJ(J+1)$, an even number $\beta'_{J_1J_2} = J_1(J_1+1) - J_2(J_2+1)$ represents the existent temporal frequency.

To found an invertible linear equation system $\boldsymbol{S} = \boldsymbol{\Gamma}\cdot\boldsymbol{\rho}$ for a finite space within $J \in [|M_0|, J_{\max}]$, valid sets of integer $\{\alpha,\beta\}$ could be chosen based on the Clebsch–Gordan coefficients and delta function in

the last equation. Alternatively, one assigns a particular set $\{\alpha, \beta\}$ for each pair $\{J_1, J_2\}$, for example $\beta = \beta'_{J_1 J_2}$ and $\alpha = J_1 + J_2$, which produce a nonsingular square coefficient matrix, and the density matrix can be retrieved as $\boldsymbol{\rho} = \boldsymbol{\Gamma}^{-1} \cdot \boldsymbol{S}$. However, such a simple choice often produces huge error for the existence of moderate noise in the observable data.

2.3. Optimal approach

The coefficient matrix $\boldsymbol{\Gamma}$ can be divided into diagonal blocks of different degenerations, where the term degeneration is defined as pairs $\{J_1, J_2\}$ having equal frequency $\beta'_{J_1 J_2}$ and the same parity sign of $(-1)^{J_1+J_2}$, and each block gives solution to the corresponding object subset $\{\rho_{J_1 J_2}\}$. In many practical cases, most off-diagonal density matrix elements are related to nondegenerate circumstances or low-degree degenerations, while the diagonals belong to the most degenerate circumstance with $\beta = 0$.

Notice that the choice of β is inalterable in a complete reconstruction, but the angular frequency for certain degeneration is still somewhat free such that the number of valid α might be more than that of related density matrix elements. More generally, the number of α employed can go beyond that necessary, and the over-determined linear equation system is solved by generalised inverse $\boldsymbol{\rho} = \boldsymbol{\Gamma}^{+} \cdot \boldsymbol{S}$, i.e. the Moore–Penrose pseudoinverse.[13,14]

Considering this alterability in the reconstruction, we provide an optimal approach in the sense of minimal error limit, by specifying the choice of angular frequencies. Concerning the transformation by a full rank rectangle matrix $\boldsymbol{\Gamma}$, an approximate error limit from the matrix analysis is

$$|\delta\boldsymbol{\rho}| \leq ||\boldsymbol{\Gamma}^{+}|| \times (|\delta\boldsymbol{S}| + ||\delta\boldsymbol{\Gamma}|| \times |\boldsymbol{\rho}|), \tag{8}$$

where $||\boldsymbol{\Gamma}^{+}|| = 1/\lambda_{\min}(\boldsymbol{\Gamma})$ is the norm of the pseudoinverse,[15] with λ the singular value.

For real molecules, perturbation $||\delta\boldsymbol{\Gamma}||$ comes from centrifugal distortion $\delta E_J \sim DJ^2(J+1)^2$ (e.g., see Ref. [7]). This term in Eq. (8) is ignored at first (to be analysed in Section 4), as the rigid rotor approximation here.

Since the error in TDMAD, mainly including the magnetic impurities, fluctuation of events counting, and, angle selective probe, Abel inversion[16] is formally complex and then transferred by the tomographic integral; it is assumed reasonably that the error δS is equally distributed along with $\{\alpha, \beta\}$. Thus, the optimisation is accomplished for each degeneration by choosing a unique set of angular frequency from the optional range confined by the triangle rule, which minimises the dominant error term $|\delta\boldsymbol{S}|/\lambda_{\min}(\boldsymbol{\Gamma})$. Then, the optimal result is obtained by the least square inversion of this selected set of 'observation'.

2.4. Fidelity

The reconstruction fidelity is measured by the normalised overlap

$$O = \frac{\mathrm{tr}[\rho_{\mathrm{pre}} \cdot \rho_{\mathrm{rec}}]}{\sqrt{\mathrm{tr}[\rho_{\mathrm{pre}}^2]\,\mathrm{tr}[\rho_{\mathrm{rec}}^2]}} \tag{9}$$

between the reconstructed and the predicted density matrices, within $O \in [0, 1]$. In a perfect reconstruction ($\rho_{\mathrm{rec}} = \rho_{\mathrm{pre}}$) this value is unity, while the overlap is zero for two orthogonal states.

3. Results

3.1. An example

The reconstruction approach is applied to deal with the typical data in Fig. 1, and the result is shown in Fig. 2, compared with the predicted density matrix.

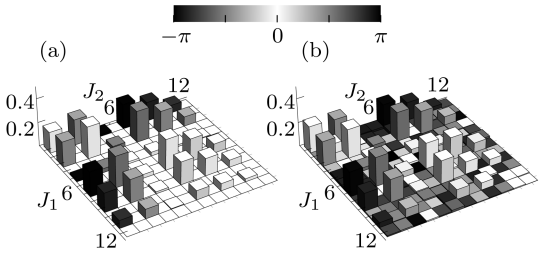


Fig. 2. (a) The density matrix of the rotational quantum state obtained in the quantum mechanics calculation, used also to simulate the data of TDMAD. (b) is the result of the optimal reconstruction approach for $J_{\max} = 12$. The quantum phase of matrix elements is represented in gray level.

Density matrix of the prepared quantum state in this example simply contains two parts (see panel (a)). The first coherent part with both odd J_1 and J_2 has major occupation due to the initial population and Raman transition. Another part is unoccupied, including a coherent portion with both J_1 and J_2 even, and zero elements with $J_1 + J_2$ odd as no transition occurs between two parities for linear rotors.

Reconstruction fidelity of this example is about 0.975 using the optimal approach, in the presence of moderate intensity of impurity and noise. In Fig. 2, a nice profile of the matrix is shown, despite that similar amplitudes of error are introduced for all elements. Significant features of the dynamically excited non-Gaussian wave packet are well retained for the populated portion. The quantum phase of elements in unoccupied positions seems seriously distorted; however, it merely influences the identification of this quantum state.

3.2. Object states

The convergence of this approach to various object states is shown in Fig. 3. Here the ratio of the occupations of object M_0 to impurity M_1 is still 9/1, and the relative noise level remains 1/2 for single detection. The sample numbers of TDMAD are determined based on a space large enough $J_{\max} = 20$, and then for each cutoff in the reconstruction the original data is re-sampled according to sampling theorem.

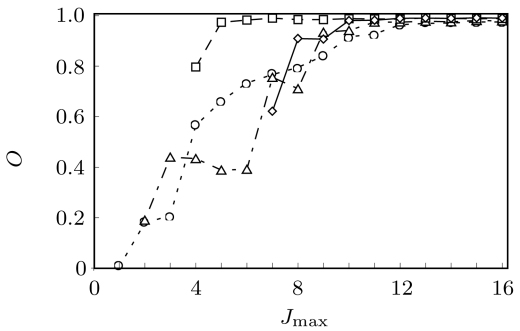


Fig. 3. The reconstruction fidelity as a function of the angular momentum cutoff, where the initial conditions of state preparation $\{M_0, M_1, J_0, I/(\mathrm{TW/cm^2})\}$ for those curves are $\{0, 1, 2, 80\}$ (circle, dotted), $\{1, 4, 5, 40\}$(triangle, dot-dashed), $\{3, 2, 3, 20\}$ (rectangle, dashed), $\{6, 3, 6, 60\}$ (diamond, solid).

Reconstruction fidelity rises up close to unity at e.g. $J_{\max} > 12$ for those object states, nearly independent of the selected magnetic subspace. No matter whether the wavepacket is broad or narrow (pumped by laser of high or low intensity), as most components are included, the fidelity becomes stable in this range. Such an adaptivity of this approach is more favourable than that in Ref. [5] where even the intensity of the pulse for excitation is limited not too weak, nor too strong to ensure the convergence. The difference is firstly attributed to the employed observable, in which TDMAD used is more sensitive to the variation of object density matrix, and this feature does not rely on the selected magnetic space, nor the concrete excitation.

The magnetic impurity might be the most important type of system noise, as the single magnetic population is created by crude techniques such as hexapole focusing (e.g. Ref. [17]) or direct cooling by supersonic expansion for nonpolar molecules. Impurities with larger $|M_0 - M_1|$ are expected to bring in more error due to greater differences of their prepared states and contribution to TDMAD, though this case might be avoided naturally in experiments where the impurity appears chiefly as the adjacent states i.e. $M_1 = M_0 \pm 1$. In general, the residual errors are very small in the converged range and are only slightly different for those magnetic states, despite the existence of several probable error sources.

4. Analysis

4.1. Norm of the inverse

The norm of the inverse matrix is a crucial factor in judging whether the transfer is robust to the perturbation of noise (refer to Eq. (8), and see also Ref. [15]). As mentioned above the optimisation is achieved by choosing one set of angular frequency for each diagonal block of the coefficient matrix individually, and it is found that the block related to the largest degeneracy with $\beta = 0$ always owns the largest error limit. Because of its broad ranged singular values and the largest number of related matrix elements, this block plays the most important role in the reconstruction fidelity.

As seen in Fig. 4, there is a bound for the norm of the pseudo-inverse of the coefficient matrix block related to $\beta = 0$, i.e. the values for $M_0 = 0$ produced from a square coefficient block for linear molecules. Along with the increase of the space scale $J_{\max}$, this value approaches a constant limit less than 6.42. The starting points for all curves are the same $\sqrt{4\pi}$ (the one-dimensional case $J_{\max} = M_0$), just the reciprocal of the maximal absolute value in $\boldsymbol{\Gamma}$, which represents a normal amplification from the tomographic integral to the density matrix. Thus, the maximal amplification is safely less than double of this factor. The reconstruction approach is always good conditioned without relation to the selected rotational subspace, as demonstrated by the favourable results in Fig. 3.

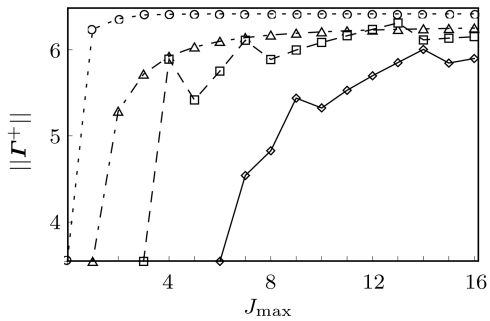


Fig. 4. The norm of the pseudo-inverse of the coefficient matrix block related to $\beta = 0$ formed in the optimal approach as a function of angular momentum cutoff. The representations for the object magnetic subspaces are the same as in Fig. 3.

4.2. Centrifugal distortion

The perturbation by centrifugal distortion[7] makes $\boldsymbol{\Gamma}$ deviate from the block diagonal matrix. As a simple estimation for this hard bond molecule, $D/B < 10^{-5}$ allows rigid rotor approximation to be within $J_{\max} \ll 10^2$ roughly. In the example in Section 3, $||\delta\boldsymbol{\Gamma}|| \simeq 0.02$, so in a noisy condition the induced error is ignored for a relatively low cutoff.

A further calculation shows that $||\delta\boldsymbol{\Gamma}||$ increases rapidly along with the cutoff $J_{\max}$, and it is only weakly dependent of varying α sets. For example, in the employed approach with higher $J_{\max} = 16$, the perturbation are $||\delta\boldsymbol{\Gamma}|| \simeq 0.10, 0.07, 0.05$ for $M_0 = 0, 1, 3$ respectively. This dependence on magnetic number might be the source of the divergences of the residual errors in Fig. 3. For a state occupied in a broad space especially with a small M_0, the rigid rotor approximation is no longer suggested. Nevertheless, the optimisation could still be defined for separate degeneration blocks as in the above, and then in the reconstruction a Γ with the distortion term surviving could be used inconsistently.

4.3. Symmetric top rotation

For symmetric top rotation in an initially selected subspace of single projection manifold (M_0 and K_0 representing the projection of J along the principal axis), the reconstruction approach defined in Section 2 can be directly applied. In this situation, the tomography is achieved by integration over Euler angle with the kernel of rotation matrix element $\langle\Omega|\alpha 00\rangle$,[9] and the second C–G coefficient in Eq. (7) is replaced by $\langle J_1 K_0 J_2 - K_0|\alpha\, 0\rangle$. Because of the similarity of K and M in the formulae, the analysis about magnetic subspace above could be extended analogously to the quantum number K. It is more advanced for $M_0 K_0 \neq 0$ (the effect of a hexapole device) that the parity selection rule vanishes, and more values of α are available in the optimisation.

5. Conclusion

In summary, we have constructed an optimal approach to retrieve a universal rotational quantum state of linear molecules, the optimisation relies only on the object rotational space concerned, being little related to experimental conditions. Reconstruction from the observable TDMAD is quite adapted for data with considerable random noise and magnetic impurity, and exhibits nice convergence for various object states. There is a small upper limit of the norm of the inverse of the coefficient matrix, showing high sensitivity of TDMAD to the rotational quantum state and a good-conditioned reconstruction, independent of specific rotational subspace.

Theoretically, from an analogous observable the idea is not yet capable to extend to an ensemble with multiple magnetic number or a broad coherent rotational state of asymmetric top, e.g. in one- or three-dimensional alignment[18,19] of this species, because the joint distribution of time and three Euler angles at most is insufficient for unique determination of its density matrix. This limit prompts to further improve the methods, such as to found complementary observables, or to define alternative solutions properly.

References

[1] Skovsen E, Stapelfeldt H, Juhl S and Mølmer K 2003 *Phys. Rev. Lett.* **91** 090406

[2] Itatani J, Levesque J, Zeidler D, Niikura H, Pépin H, Kieffer J C, Corkum P B and Villeneuve D M 2004 *Nature* **432** 867

[3] Hasegawa H and Ohshima Y 2008 *Phys. Rev. Lett.* **101** 053002

[4] Mouritzen A S and Mølmer K 2006 *J. Chem. Phys.* **124** 244311

[5] Deshpande S A and Ezra G S 2007 *Chem. Phys. Lett.* **440** 341

[6] Torres R, de Nalda R and Marangos J P 2005 *Phys. Rev.* A **72** 023420

[7] Hamilton E, Seideman T, Ejdrup T, Poulsen M D, Bisgaard C Z, Viftrup S S and Stapelfeldt H 2005 *Phys. Rev.* A **72** 043402

[8] Rosca-Pruna F and Vrakking M J J 2001 *Phys. Rev. Lett.* **87** 153902

[9] Gordy W and Cook R L 1984 *Microwave Molecular Spectra* (3rd ed) (New York: Wiley Interscience) pp11–35

[10] Guo C, Li M, Nibarger J P and Gibson G N 1998 *Phys. Rev.* A **58** R4271

[11] Tong X M, Zhao Z X and Lin C D 2002 *Phys. Rev.* A **66** 033402

[12] Guo W, Zhu J Y, Wang B X, Wang Y Q and Wang L 2008 *Phys. Rev.* A **77** 033415

[13] Rao C R and Mitra S K 1972 *Proceedings of the Sixth Berkeley Symposium on Mathematical Statistics and Probability* (Vol. 1) Berkeley, United States of America, 1970 pp601–620

[14] Opatrný T, Welsch D-G and Vogel W 1997 *Phys. Rev.* A **56** 1788

[15] Sun J G 1987 *Matrix Perturbation Analysis* (Beijing: Science Press) p355 (in Chinese)

[16] Bordas C, Paulig F, Helm H and Huestis D L 1996 *Rev. Sci. Instrum.* **67** 2257

[17] Anderson R W 1997 *J. Phys. Chem.* A **101** 7664

[18] Péronne E, Poulsen M D, Bisgaard C Z, Stapelfeldt H and Seideman T 2003 *Phys. Rev. Lett.* **91** 043003

[19] Underwood J G, Sussman B J and Stolow A 2005 *Phys. Rev. Lett.* **94** 143002